SYNERGISTIC FLOW INDUCED MOTION OF TWO CYLINDERS HARVESTING MARINE HYDROKINETIC ENERGY

Michael M. Bernitsas[1] Hai Sun
Marine Renewable Energy Laboratory
Univ. of Michigan; and Vortex Hydro Energy
Ann Arbor, MI, USA

Erik Mauer
Allegheny Science & Technology
Contractor to US-DOE

Gary Nowakowski
US-DOE, Wind and Water Power Technologies Office,
Golden , CO, USA

[1]Corresponding author: michaelb@umich.edu

ABSTRACT

In transverse flow, cylinders respond in FIM (Flow Induced Motions); particularly VIV (Vortex Induced Vibrations) and galloping. Both are driven by alternating lift and result in oscillatory motion. Alternating Lift Technologies (ALT) [1] provide an environmentally compatible way of harnessing hydrokinetic energy even from slow flows, starting at 0.4 m/s. [2]. The VIVACE (VIV for Aquatic Clean Energy) Converter uses multiple cylinders, in tandem, with distributed surface roughness, on elastic supports. Experiments are conducted with two cylinders in FIM. With hydrodynamic synergy, they can harness 2.56-7.5 times more hydrokinetic power than two isolated cylinders responding to the same flow velocity.

1. INTRODUCTION

Rigid cylinders on elastic supports in transverse flows can be managed in FIM, converting Marine Hydrokinetic (MHK) energy to mechanical and electrical energy. VIV and galloping are the most commonly occurring FIM and are implemented in the VIVACE Converter mechanics [3,4]. An important question in the Fluid-Structure Interaction (FSI) mechanics of this ALT converter is how close cylinders can be placed to achieve highest hydrokinetic energy conversion. This metric affects directly the power-to-volume density. Fish in schools move effortlessly by proper placement in the wake of fish ahead of them [5]. VIVACE is being developed to achieve optimal FSI synergy among cylinders organized in a school to capture the energy within a volume of flow like a true 3-D converter.

Multi-cylinder tests have been conducted in the Low Turbulence Free Surface Water (LTFSW) Channel in the Marine Renewable Energy Laboratory (MRELab) at the University of Michigan [6,7] for Reynolds numbers in the range $30{,}000 \leq Re \leq 120{,}000$, which falls in the high-lift TrSL3 flow regime [8]. Results show that synergy of FSI for four cylinders can produce power as much as 80% greater than four cylinders in isolation [7]. In this paper, a more systematic study is initiated to establish this breakthrough discovery starting with two cylinders in tandem. Damping and stiffness are used as parameters to optimize the power output. Mass ratio is also considered. Distributed roughness in the form of roughness strips is applied to accelerate the onset of galloping and, thus, increase the harnessed MHK power across the range of flow velocities over which VIVACE is designed to operate. The recently developed second generation of virtual spring-damping system, V_{ck}, in the MRELab enables embedded computer-controlled change of viscous-damping and spring-stiffness for precise oscillator modeling and fast parameter changes for systematic testing [9]. Experimental results for harvested power and the supporting data on amplitude response are presented for two cylinders in tandem and compared to the corresponding information for a single-cylinder (that is, single oscillator) Converter [10].

2. PHYSICAL MODEL

A VIVACE Converter consists of a single circular cylinder suspended on end-springs, mass, damping, and a power take-off (PTO) system. The physical model consists of two oscillators simulated by the Vck with distributed surface roughness applied to the cylinders [4, 11].

2.1. Experimental Facility: LTFSW Channel

Tests were conducted in the LTFSW Channel, in the MRELab. The Channel recirculates 37,854lt of fresh water at speed up to 1.5m/s using an impeller powered by a 20hp induction motor. The test section is 2.44m long, 1.0m wide, and made of transparent plexi-glass, enabling visualization of flow using two 5W argon lasers & Al_2O_3 particles of 100μm. The water depth was set at 1.17m and the flow speed limited to 1.35 m/s for safety from galloping. Figure 1, shows a two-oscillator system in the Channel.

FIGURE 1. TWO-CYLINDER VIVACE CONVERTER WITH V_{CK} IN THE LTFSW CHANNEL

2.2. Cylinders and distributed roughness

The excitation comes from the fluid-structure interaction (FSI) and is applied on the cylinder. To enhance FIM of cylinders, to harness more MHK energy, distributed roughness in the form of roughness strips was introduced and extensively studied in the MRELab experimentally [4] and numerically [6]. Study of the distributed roughness, termed Passive Turbulence Control (PTC), resulted in the *PTC-to-FIM Map* [11]. PTC location determines the FIM type. Placement angle α_{PTC}=20°, is measured from the fore stagnation point to the strip edge. P60 strips of 12.7mm width, covering 16° were used on each side of the 88.9mm diameter cylinder (Table 1).

TABLE 1. OSCILLATOR PARTICULARS	
L/D	1.57, 2.0, 2.57
k [N/m]	400 ~ 1,200
Temp. (^{0}C)	18.5~20.5
μ [Ns/m^2]	1.004E-03
ρ [kg/m^3]	999.729
D [m]	0.0889
L [m]	0.895
m_{disp}(kg)	5.425
$m_{oscillation}$ (kg)	7.286-
$m^*=m_{osc}/m_{disp}$	1.343,
m_{added} (kg)	5.425
$\zeta_{structure}$	0.020
$f_{n,water}$	0.97 ~ 1.67

2.3. Oscillator simulated by the Vck system

For systematic experimental testing particularly in such a large design space, two challenges are important to overcome: (a) Changing the physical springs and dampers requires extensive calibration and alignment time. (b) The viscous damping of the system is rarely linear as modeled in classical vibration textbooks. To compensate for these two major challenges, MRELab developed the embedded 2nd generation V_{ck} in model oscillators [9]. V_{ck} replaces the physical oscillator with a simulator without including the hydrodynamics in the closed control loop, which would bias the FIM measured.

2.4. Math model for a V_{ck} VIVACE system

Based on the non-linear viscous damping model, the controller force can be expressed as:

$$F_{controller} = F_{nonlinear\_damping} - c_{virtual}.\dot{y} - K_{virtual}.y \quad (1)$$

where $F_{controller}$ is the force applied by the virtual system, $F_{nonlinear\_damping}$ is the total nonlinear damping force, $K_{virtual}$ is the virtual spring constant. $c_{virtual}$ is the virtual linear viscous damping added after subtracting the nonlinear viscous damping so that the system tested is a mathematically-true linear damping system. The agreement between the real spring system and V_{ck} system is excellent in VIV and galloping tests over the entire range of Channel velocities [9].

3. MATHEMATICAL MODEL OF CONVERTED POWER

The flow direction is x; the cylinder motion is in the vertical y-direction. FIM is modeled as

$$m_{osc}.\ddot{y} + c_{total}.\dot{y} + ky = F_{Fluid}.\hat{y} \quad (2)$$

where m_{osc} is the total oscillating system mass, including one third of the spring mass, k is the spring stiffness, c_{total} is the total damping coefficient, and F_{Fluid} is the force exerted by the fluid on the body in the y-direction. In order to convert hydrokinetic energy to mechanical energy in the oscillator and subsequently electrical energy, additional damping is introduced into the system. The total damping c_{total} is defined as

$$c_{total} = c_{structure} + c_{harness} \quad (3)$$

where $c_{structure}$ is the friction losses in the transmission system, and $c_{harness}$ is the damping added through V_{ck} to convert the mechanical energy in the oscillating cylinder to electrical. $c_{structure}$ and $c_{harness}$ can be expressed using damping ratio $\zeta_{harness}$ and $\zeta_{structure}$, respectively.

$$\zeta_{structure} = \frac{c_{structure}}{2\sqrt{(m_{osc}+m_a)K}} \quad (4) \qquad \zeta_{harness} = \frac{c_{harness}}{2\sqrt{(m_{osc}+m_a)K}} \quad (5)$$

The mechanical power in VIVACE is expressed as:

$$P_{VIVACE-Mech} = \frac{1}{T_{osc}}\int_0^{T_{osc}} 4\pi(m_{osc}+m_a)\zeta_{total}\dot{y}^2 f_{n,water}\,dt \quad (6)$$
$$= 8\pi^3(m_{osc}+m_a)\zeta_{total}(Af_{osc})^2 f_{n,water}$$

The harnessed power is

$$P_{VIVACE-harness} = 8\pi^3(m_{osc}+m_a)\zeta_{harness}(Af_{osc})^2 f_{n,water} \quad (7)$$

and can be recast as

$$P_{VIVACE-harness} = \frac{1}{2}c_{harness}A^2\omega_{osc}^2 \quad (8)$$

where, A is the amplitude of oscillation, and ω is the angular frequency. Similar expressions can be written for the dissipated power and the total converted power.

4. RESULTS AND DISCUSSION

The cylinder displacement as a function of time is recorded using the motor encoder. The acquired data are post-processed using Equations (1)-(8). Only the following are presented in this paper:

(a) The cylinder amplitude A, calculated by averaging the absolute values of the 60 highest positive or negative peaks in 60s run time.

(b) The harnessed power, calculated by Eq. (8), and the total converted power.

They are plotted versus *Re*, reduced velocity U^*, and flow velocity *U*. Tested cases are summarized in Table 1. Presentation is limited to two cylinders in tandem with center-to-center spacing L/D=1.57, *k*=1,200N/m, and parameter $\zeta_{harness}$.

The stiffness *k* selected is accurate in form and value and exact, set by the calibrated motor-torque and its relation to rotation. That is, *k* is not subjected to fabrication error or fatigue degradation in time. Similarly, $\zeta_{harness}$ *and* ζ_{total} are exact and really linear viscous as explained in the discussion for the V_{ck} system [9]. The *Re* and U^* ranges are $3\bullet10^4 \le Re \le 1.2\bullet10^5$ and $2.92 \le U^* \le 15.33$.

4.1. Single Cylinder Results

Results, specifically converted power and *A/D*, should be compared to the corresponding isolated cylinder results shown in Figs. 2-3 [10].

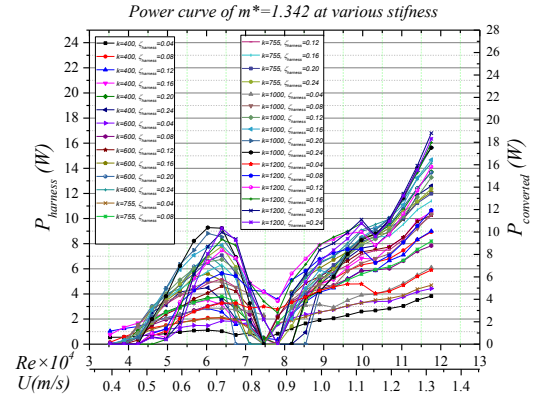

FIGURE 2. POWER CURVES OF SINGLE-CYLINDER CONVERTER FOR m^*=1.343; *k* AND $\zeta_{harness}$ AS PARAMETERS

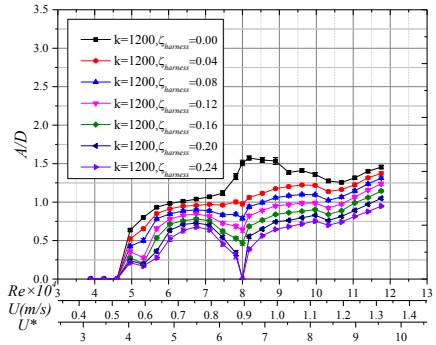

FIGURE 3. RESPONSE AMPLITUDE FOR m^*=1.343 WITH *k*=1,200N/M AND $\zeta_{harness}$ AS PARAMETER

4.2. Amplitude Response

The VIVACE oscillators are not linear. Their response actually is composed of two nonlinear phenomena, VIV and galloping, positioned back-to-back via the distributed surface roughness (PTC) to achieve broad-band, large-amplitude response. In contrast, linear oscillators exhibit large response only over a narrow band around the natural frequency. The various branches are discussed as shown in the isolated cylinder (Figs. 2-3) or the two cylinders in tandem (Figs. 4-9).

4.2.1. Upstream Cylinder (Figure 4)

(a) $30{,}000 \le Re \le 45{,}000 \sim 50{,}000$: This is the initial branch of VIV. A drop in *A/D* can be observed from $\zeta_{harness}$=0.00 to $\zeta_{harness}$=0.24. This is due to the added damping for energy harnessing

(b) $45{,}000 \le Re \le 65{,}000$ is the upper branch of VIV. The upper branch is narrower than the isolated cylinder in Figure 3. The close spacing disturbs the vortex structures.

(c) $68{,}000 \sim 70{,}000 \le Re \le 80{,}000 \sim 90{,}000$: This is the lower branch of VIV, desynchronization, the gap between VIV and galloping, and the onset of galloping. Not all four sub-ranges are obvious in all amplitude curves, because the VIV range moves with changes in *k* and shrinks with increasing $\zeta_{harness}$. On the contrary, the onset of galloping moves to higher velocities with increasing $\zeta_{harness}$. As $\zeta_{harness}$ increases, desynchronization becomes more obvious for all *k* values. In this region, which includes all four sub-ranges, the amplitude drops dramatically and random oscillatory patterns appear as expected. Consequently, the error bars become significantly larger.

(d) $80{,}000 \sim 90{,}000 \le Re$: This is the galloping region. Galloping is a high-amplitude and low-frequency FIM instability due to asymmetry. Non-circular cross-section cylinders could be subjected to high amplitude galloping oscillation due to their geometric asymmetry with respect to the flow. In this region, the upstream cylinder is affected by the downstream cylinder at this close spacing.

4.2.2. Downstream cylinder (Figure 5)

(a) $30{,}000 \le Re \le 45{,}000 \sim 50{,}000$: Is the initial branch of VIV, despite the amplitude response not showing typical features. Strong suppression is observed. For *L/D*=1.57 and *k*=1,200N/m, suppression reaches up to *Re*=55,000. Suppression increases as *k* and $\zeta_{harness}$ increase.

(b) $45{,}000 \sim 50{,}000 \le Re \le 80{,}000$: Upper branch and transition region. A lower branch appears at this high stiffness even for high damping. The amplitude is higher than the upstream cylinder for $0.12 < \zeta_{harness}$, showing that the downstream cylinder is effected by the upstream more in higher damping.

(c) 80,000≤*Re*: Galloping, where the response is nearly that of the isolated cylinder (Fig. 4).

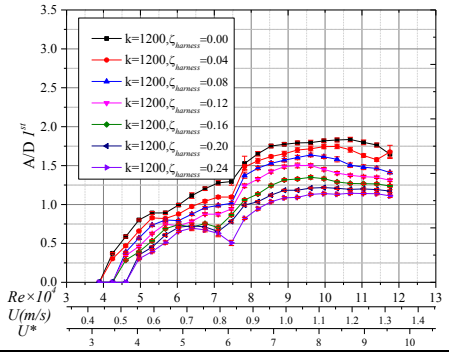

FIGURE 4. FIM AMPLITUDE RESPONSE OF UPSTREAM CYLINDER

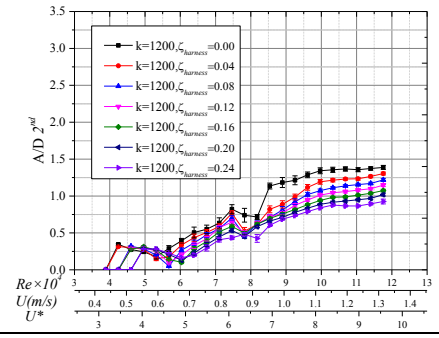

FIGURE 5. FIM AMPLITUDE RESPONSE OF DOWNSTREAM CYLINDER

4.3. Converted Power

The experimental results are shown in Figures 6-9 for the 1st, 2nd, both, and isolated cylinder, respectively. The right *y*-axis is the scale for the total converted power, which includes both the harnessed power and the dissipated power.

(a) 38,000<*Re*<70,000~75,000: This region contains the VIV initial branch and VIV upper branch. A steady growth of power can be observed. For an isolated cylinder (Figure 2), softer spring stiffness, with lower harness damping ratio, initiate power harness at flow velocity as low as 0.3946 m/s. The same is true for all spacings for two cylinders, though results are not shown due to space constraints.

(b) 68,000~70,000≤*Re*≤80,000~82,000: This region is past the VIV upper branch to VIV lower branch to desynchronization. The harnessed power maintains a steady growth for L/D=1.57.

(c) 80,000~82,000≤*Re*: This is transition followed by galloping. Harnessed power increases as the flow velocity increases, regardless of the damping ratio. The highest harnessed power of two tandem cylinders is 42.1W at L/D=1.57. Compared to the highest harnessed power of a single cylinder (16.8W), it is 2.5 times higher.

Table 2 shows that two cylinders in synergy generate 2.56-7.5 times the power of an isolated cylinder. This is a major breakthrough conclusion in design of multi-cylinder converters.

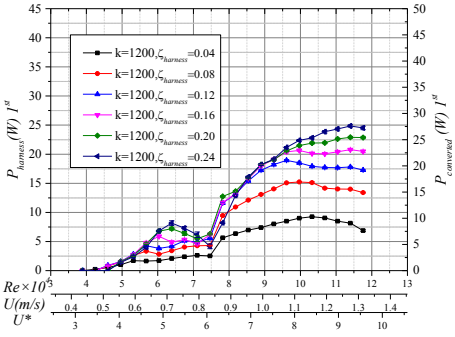

FIGURE 6. POWER CONVERTED AND HARNESSED BY UPSTREAM CYLINDER

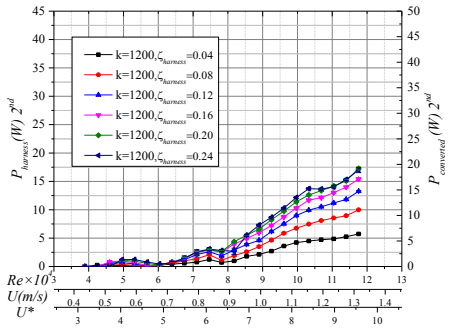

FIGURE 7. POWER CONVERTED AND HARNESSED BY DOWNSTREAM CYLINDER

TABLE 2. POWER OF TWO CYLINDERS IN SYNERGY VS. AN ISOLATED CYLINDER; *k*=1,200N/m, $\zeta_{harness}$=0.24

U_{flow} [m/s]	Converted Power [Watts]				
	1st Cyl.	2nd Cyl.	Synergy	Isolated	Ratio
0.90	12	3	15	2.0	7.5
1.00	20	8.5	28.8	7.5	3.84
1.10	24	12.5	36.5	10.0	3.65
1.23	27	16.0	43.0	13.0	3.31
1.28	27	17.0	44.0	15.5	2.84
1.32	27.5	18.5	46.0	18	2.56

4.4. Interaction Phenomena

Figs. 10-11 provide qualitative information in understanding cylinder interaction. Depending on the cylinder spacing and the flow velocity, the vortices and shear layers from the upstream cylinder reach the downstream cylinder at different phases of vortex growth on the rear cylinder. Fig. 10 shows the case of suppression of the rear cylinder VIV at Re=30,000. Timing of upstream vortices hitting the 2nd cylinder is such that they grab the same rotation vortices from the 2nd cylinder leaving it without circulation and lift. VIV of 2nd cylinder is suppressed with negative effects on power conversion. On the contrary, at *Re*=90,000, the two cylinders are nearly in phase in VIV to galloping transition. Partial vorticity coalescence occurs increasing lift in the second cylinder as the VIV mechanism is in phase with the galloping instability. Amplitude *A*>2.5**D*.

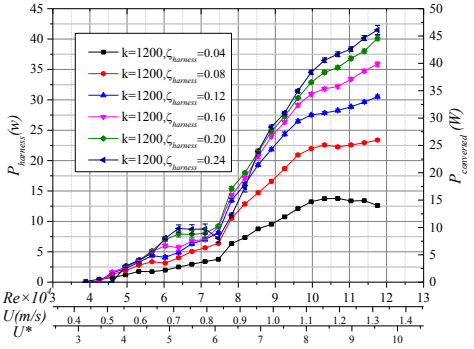

FIGURE 8. POWER CONVERTED AND HARNESSED BY TWO CYLINDERS IN TANDEM

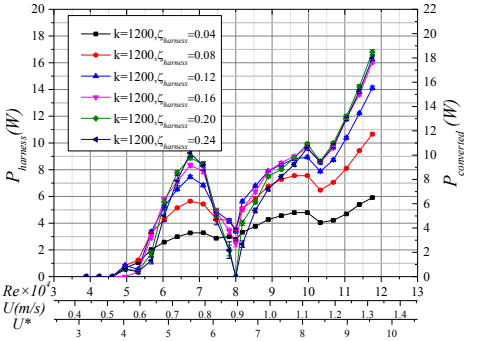

FIGURE 9. POWER CONVERTED AND HARNESSED BY SINGLE ISOLATED CYLINDER

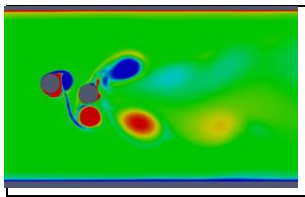

FIGURE 10. Re=30,000; VIV OF REAR CYLINDER IS SUPPRESSED [6]

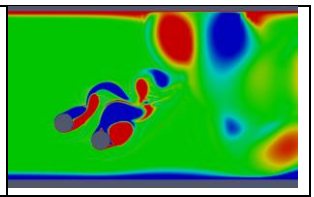

FIGURE 11. RE=90,000; GALLOPING OF REAR CYLINDER IS ENHANCED [6]

CONCLUSIONS

- Two cylinders in tandem can undergo FIM synergistically to harness 2.56-7.5 more MHK energy in a school than in isolation.
- The MHK power harnessed by the upstream cylinder is increased by up to 100%, affected by the downstream cylinder.
- The MHK power harnessed by the downstream cylinder and its FIM are affected to a lesser extent by the upstream cylinder.
- VIVACE can harness energy from flows as slow as 0.3946 m/s with no upper limit.
- Close spacing and high spring stiffness combined yield highest harnessed power.
- Local power maxima exist at the end of the VIV upper branch and the highest galloping velocity.

ACKNOWLEDGEMENTS

Prepared under Cooperative Agreement No. DE-EE0006780 between Vortex Hydro Energy, Inc. and the U.S. Department of Energy. The MRELab is a subcontractor through the University of Michigan.

Prepared as an account of work sponsored by an agency of the US Government. Neither the US Government nor any agency thereof, nor any of their employees, makes any warranty, express or implied, or assumes any legal liability or responsibility for the accuracy, completeness, or usefulness of any information, apparatus, product, or process disclosed, or represents that its use would not infringe privately owned rights. Reference herein to any specific commercial product, process, or service by trade name, trademark, manufacturer, or otherwise does not necessarily constitute or imply its endorsement, recommendation, or favoring by the US Government or any agency thereof. The views and opinions of authors expressed herein do not necessarily state or reflect those of the US Government or any agency thereof.

REFERENCES

[1] Bernitsas, M. M., 2016, "Harvesting Energy by Flow Included Motions", Chapter 47, Springer Handbook of Ocean Engineering, Editors: Dhanak, M. R., Xiros, N. I., Springer-Verlag Berlin Heidelberg.

[2] Lacey, R.W.J, Neary, V.S., Liao, J.C., Enders, E.C., Tritico, H.M., 2011, "The Ipos Framework: Linking Fish Swimming Performance in Altered Flows from Laboratory Experiments to Rivers", River Research.

[3] Bernitsas M.M., Raghavan K., 2009 "Converter of Current, Tide, or Wave Energy", US Patent and Trademark Office, Patent# 7,493,759 B2, Feb. 24.

[4] Bernitsas, M. M. and Raghavan, K., 2011, "Enhancement of Vortex Induced Forces & Motion through Surface Roughness Control" US Patent and Trademark Office, Patent# 8,047,232 B2, Nov. 1.

[5] Wolfgang, M.J., Anderson, J.M., Grosenbaugh, M.A., Yue, D.P.K., Triantaphyllou, M.S., 1999, "Near Body Flow Dynamics in Swimming Fish", Experimental Biology, Vol. 202, 1999, pp.2303-2327.

[6] Ding, L., Zhang L., Kim E.S., Bernitsas, M.M., "2D-URANS vs. Experiments of Flow Induced Motions of Multiple Circular Cylinders with Passive Turbulence Control", Journal of Fluids and Structures, Vol. 54, 2015, pp. 612-628.

[7] Kim,E.S., Bernitsas, M.M., "Performance prediction of horizontal hydrokinetic energy converter using synergy of multiple cylinders in flow induced motion", Applied Energy 170 (2016) 92–100.

[8] Zdravkovich, M. M., (1997a), "Flow Around Circular Cylinders, Vol. 1", E. Achenbach, ed., Oxford University Press, Oxford, UK.

[9] Sun, H., Bernitsas, M. P., Kim, E. S., Bernitsas, M. M., "Virtual Spring-Damping System for Fluid Induced Motion Experiments", J. of Offshore Mechs. & Arctic Engnrg., ASME Trans, Dec. 2015, 137,1, 061801.

[10] Sun, H., Kim. E. S., Nowakowski, G., Mauer, E., Bernitsas, M.M., 2016, "Effect of Mass-Ratio, Damping, and Stiffness on Optimal Hydrokinetic Energy Conversion of a Single, Rough Cylinder in Flow Induced Motions", Renewable Energy, 2016.

[11] Park, H.R., Kumar, R.A., Bernitsas, M.M., 2013, "Enhancement of Flow Induced Motions of Rigid Circular Cylinder on Springs by Localized Surface Roughness at $3\times10^4 \le Re \le 1.2\times10^5$", Ocean Engineering, 72, 1 Nov., 403-415.